Electronic Supplementary Material (ESI) for RSC Advances.
This journal is © The Royal Society of Chemistry 2015

Supporting Information

Sequential detection of mercury (II) and thiol-containing amino acids by a fluorescent chemosensor

Ga Rim You, Sun Young Lee, Jae Jun Lee, Yong Sung Kim, Cheal Kim*

Department of Fine Chemistry and Department of Interdisciplinary Bio IT Materials, Seoul National University of Science and Technology, Seoul 139-743, Korea. Fax: +82-2-973-9149; Tel: +82-2-970-6693; E-mail: chealkim@seoultech.ac.kr

(a)

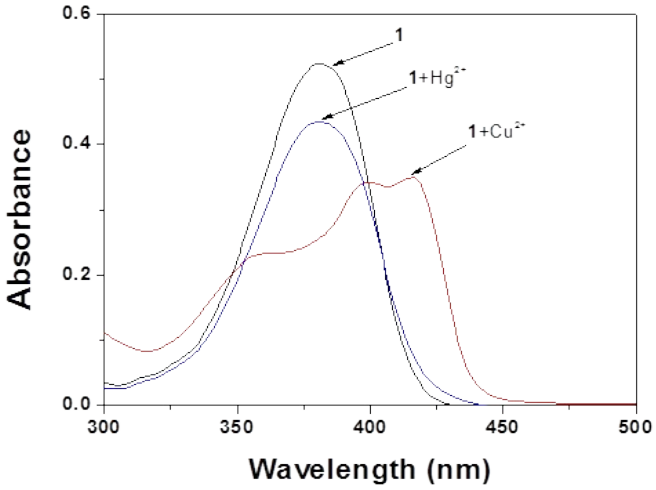

(b)

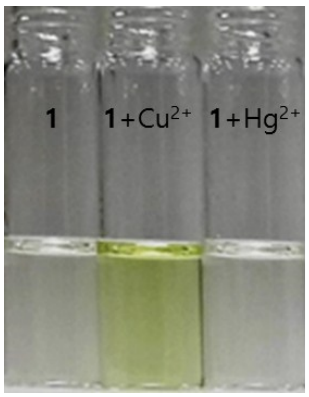

Fig. S1 (a) Changes in the UV-vis spectra of receptor **1** (10 μM) upon addition of Cu^{2+} (1 equiv) and Hg^{2+} (1 equiv), respectively, in DMSO/bis-tris buffer (8/2, v/v). The bathochromic shift of **1**-Cu^{2+} complex might be explained through the internal charge transfer (ICT) and ligand-to-metal charge-transfer (LMCT) in the molecule, which has the push-pull effect of the electron-donating and the electron-withdrawing group. Therefore, **1**-Cu^{2+} complex showed a color change, whereas **1**-Hg^{2+} complex did not. (b) The color changes of **1** (30 μM) upon the addition of Cu^{2+} (1 equiv) and Hg^{2+} (1 equiv), respectively, in DMSO/bis-tris buffer (8/2, v/v).

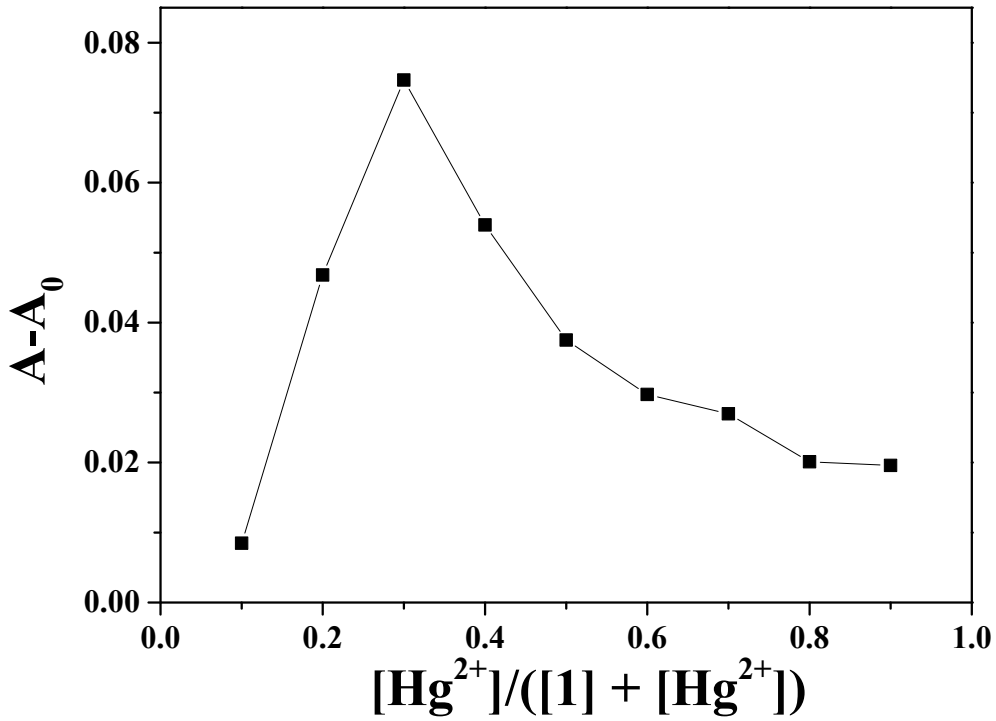

Fig. S2 Job plot for the binding of **1** with Hg^{2+}. Absorbance at 385 nm was plotted as a function of the molar ratio $[Hg^{2+}]/([\mathbf{1}] + [Hg^{2+}])$. The total concentrations of mercury ions with receptor **1** were 30 μM.

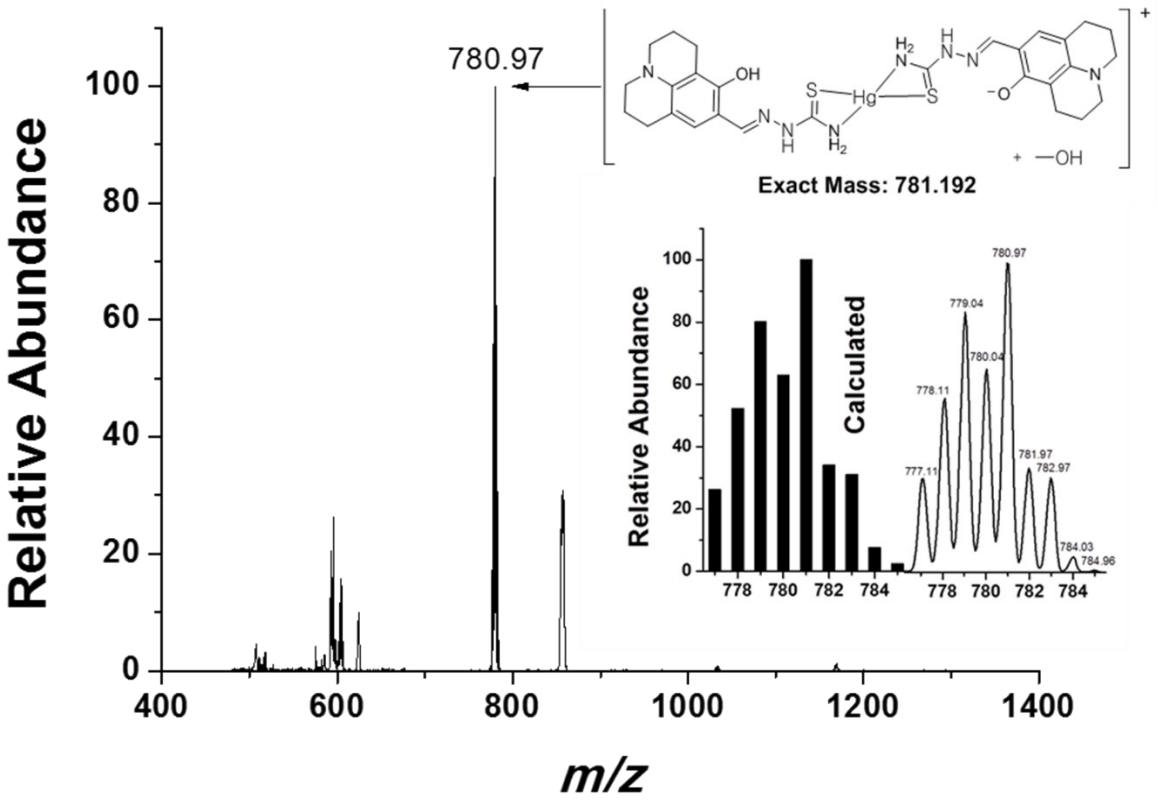

Fig. S3 Positive-ion electrospray ionization mass spectrum of **1** (100 μM) upon addition of 1 equiv of $Hg(NO_3)_2$.

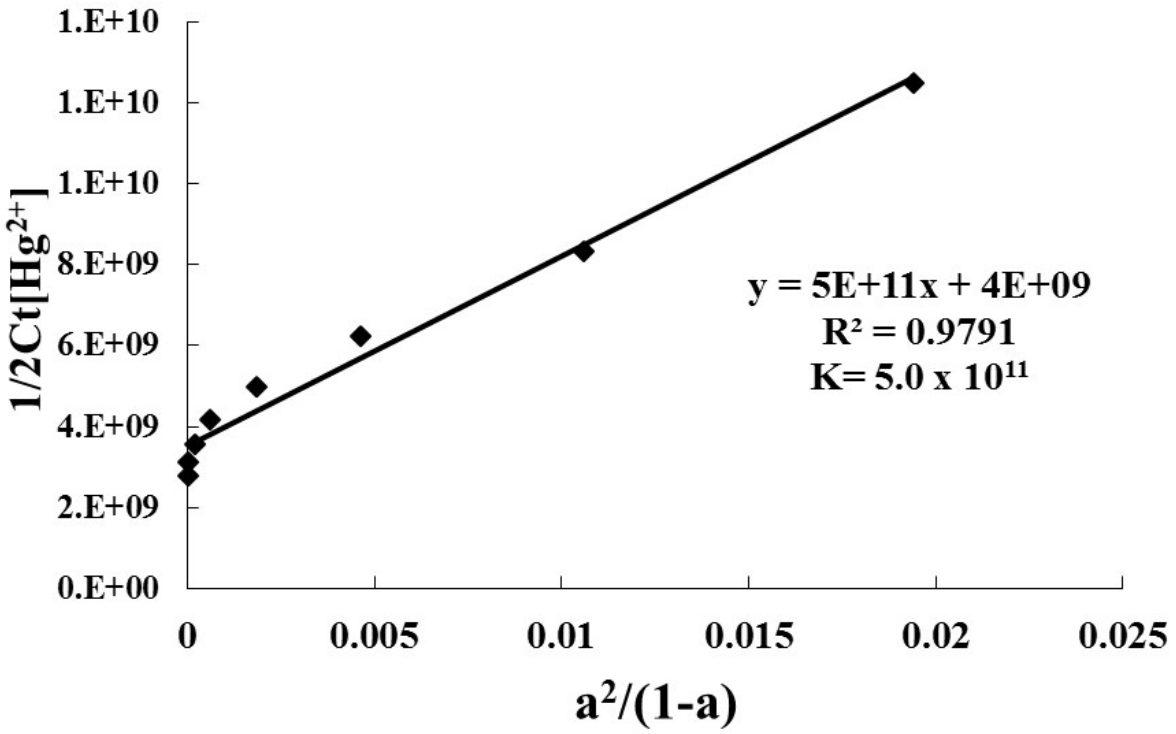

Fig. S4 Li's equation plot (absorbance at 382 nm) of **1**, assuming 1:2 stoichiometry for association between Hg^{2+} and **1**. 'Ct' means the concentration of **1**, and 'a' does $[(A_x-A_{max})/(A_0-A_{max})]$.

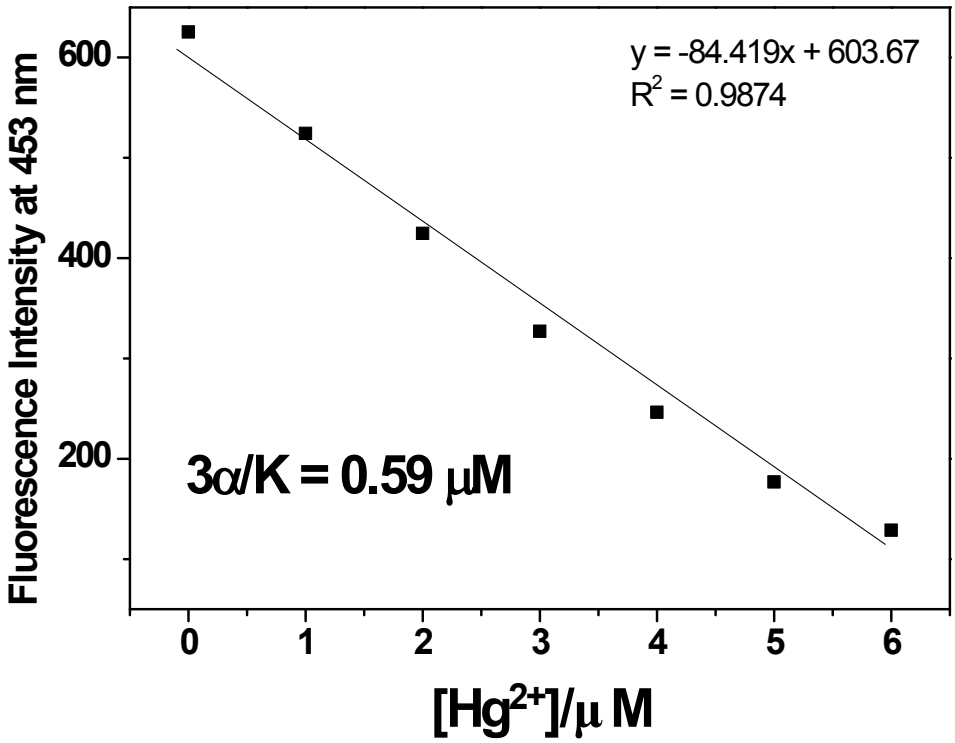

Fig. S5 Determination of the detection limit based on change in the ratio (absorbance at 453 nm) of **1** (10 μM) with Hg^{2+}.

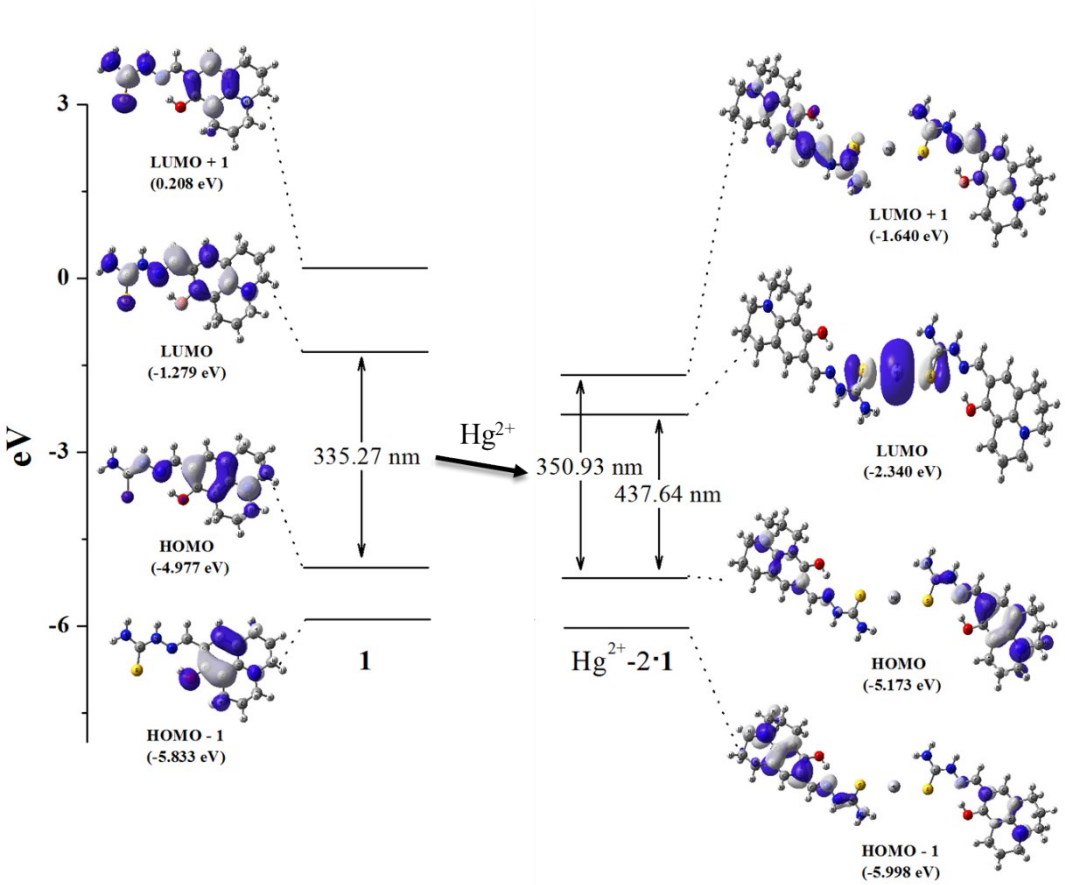

Fig. S6 Frontier molecular orbitals and their energies of **1** and Hg^{2+}-2·**1** complex.

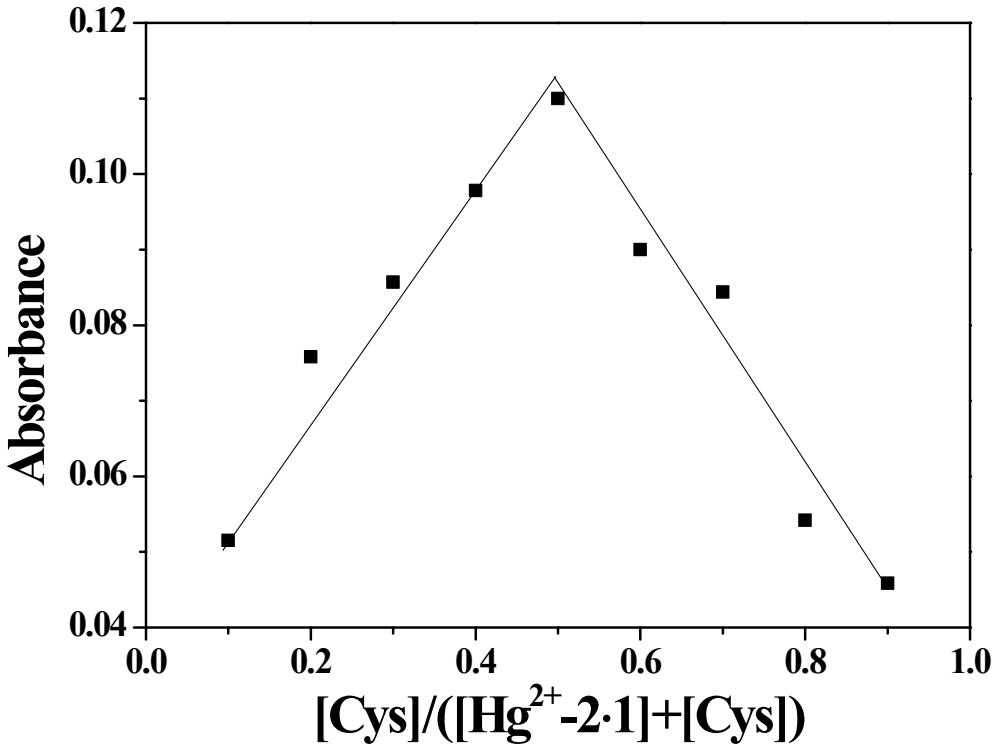

Fig. S7 Job plot for the binding of Hg^{2+}-2·**1** with Cys. Absorbance at 382 nm was plotted as a function of the molar ratio [Cys]/([Hg^{2+}-2·**1**] + [Cys]). The total concentrations of Cys with Hg^{2+}-2·**1** were 10 μM.

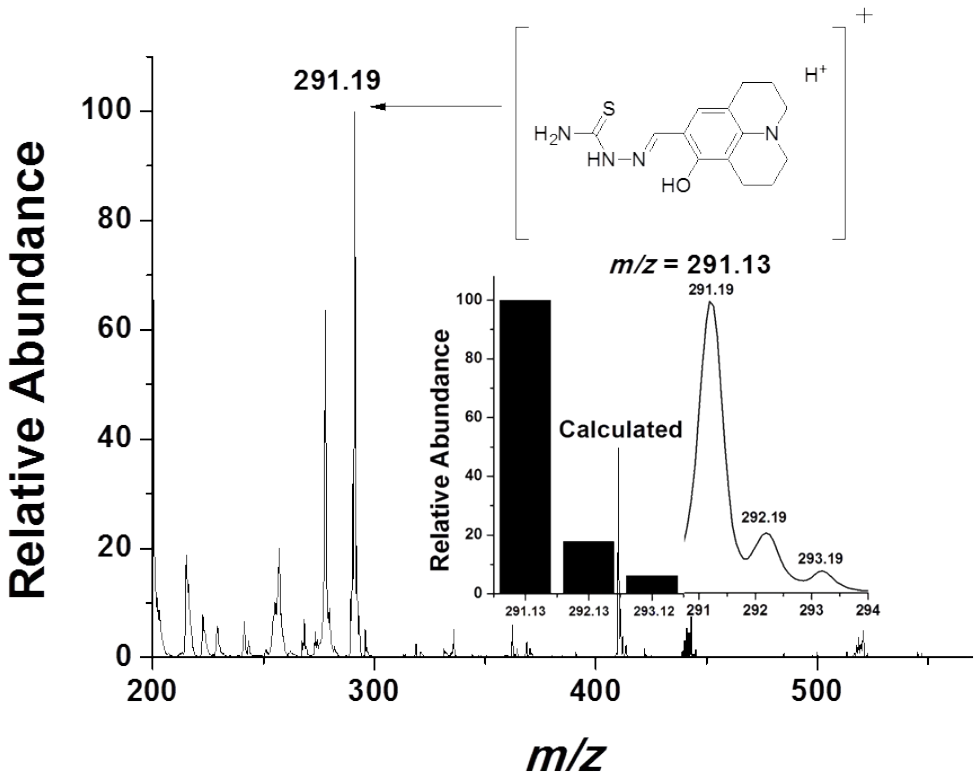

Fig. S8 Positive-ion electrospray ionization mass spectrum of Hg^{2+}-2·**1** (100 μM) upon addition of 1 equiv of Cys.

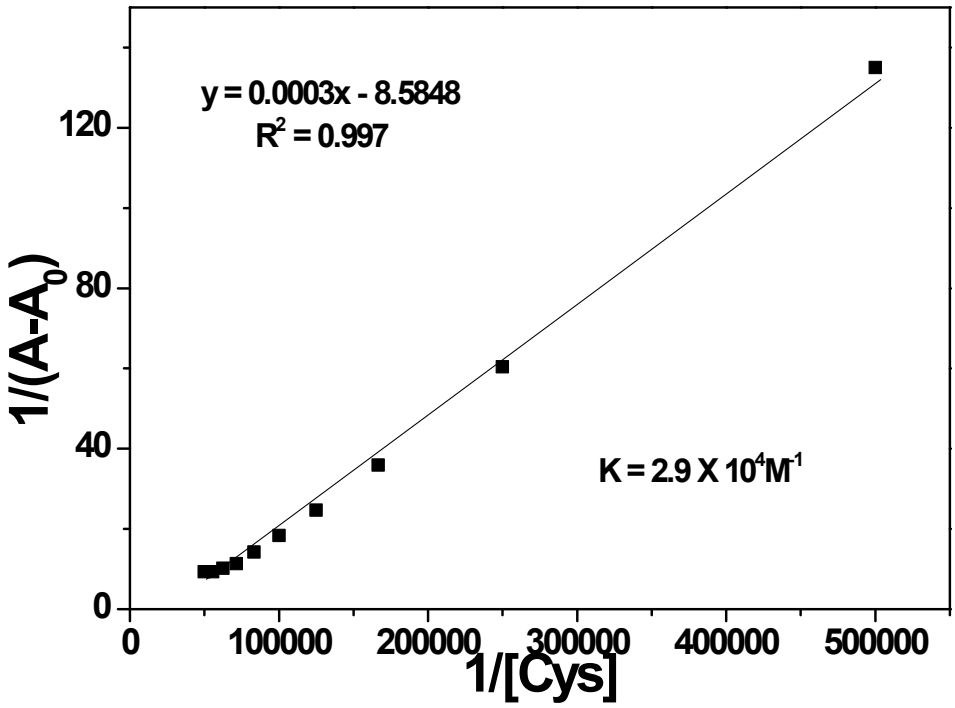

Fig. S9 Benesi-Hildebrand plot (absorbance at 382 nm) of **1**, assuming a 1:1 stoichiometry for association between **1** and Hg^{2+}.

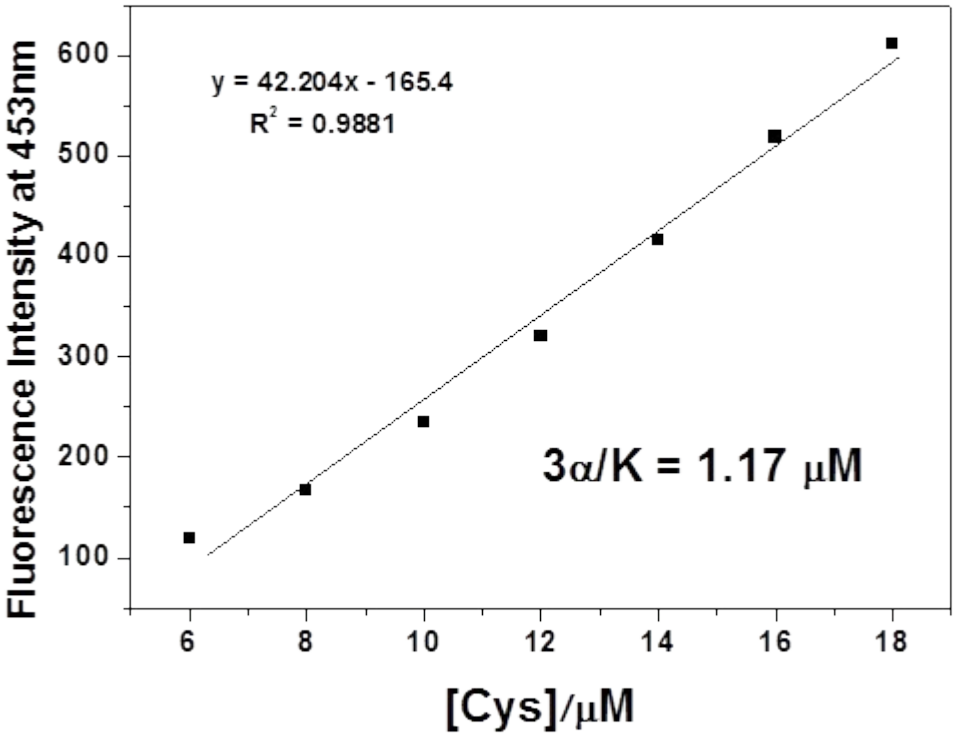

Fig. S10 Determination of the detection limit based on change in the ratio (absorbance at 453 nm) of Hg^{2+}-2·**1** (10 μM) with Cys.

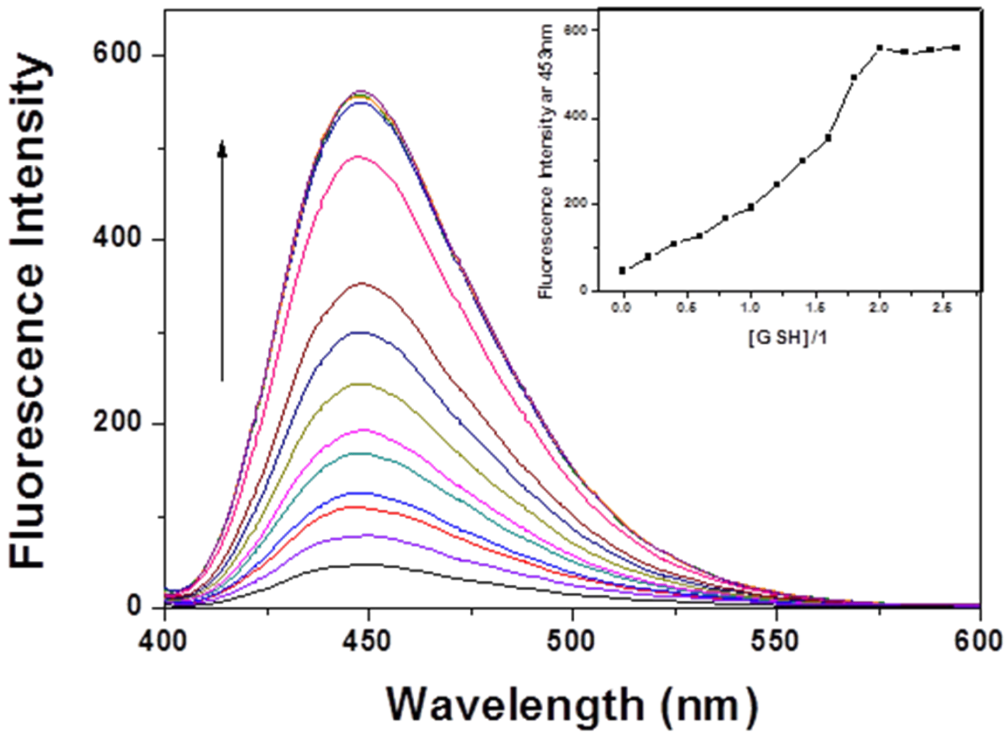

Fig. S11 Fluorescence spectral changes of Hg^{2+}-2·**1** in the presence of different concentrations of GSH in DMSO/bis-tris buffer (8/2, v/v). Inset: Fluorescence intensity at 453 nm versus the number of equiv of GSH added.

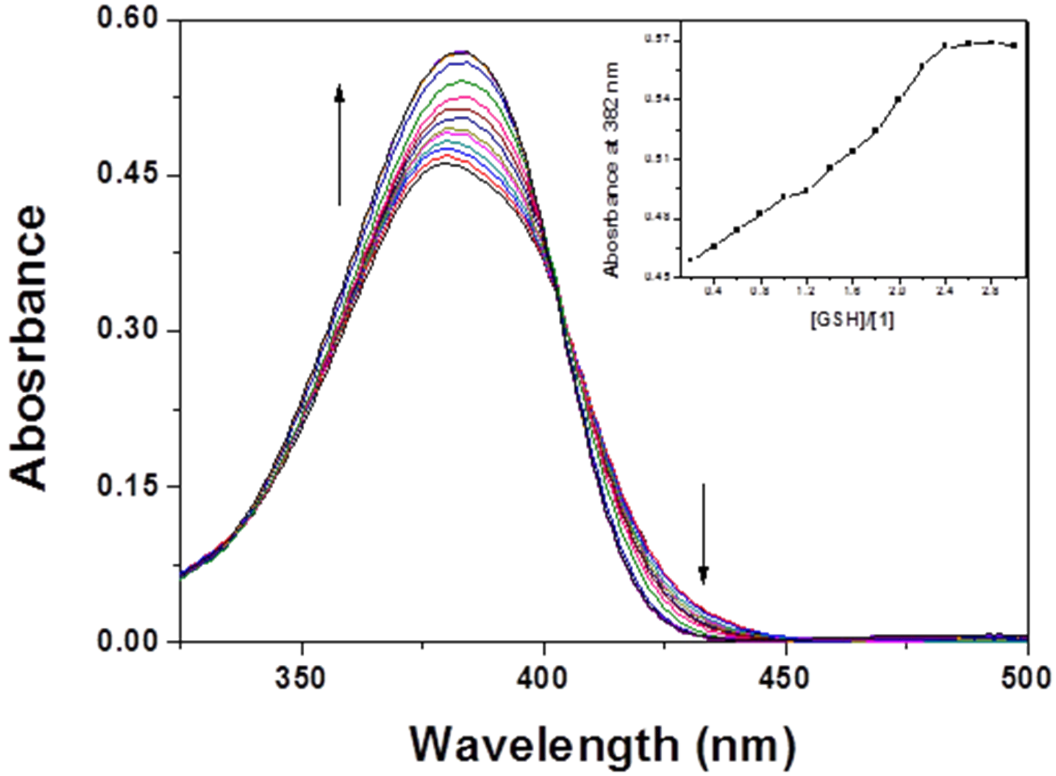

Fig. S12 Absorption spectral changes of Hg^{2+}-2·**1** after addition of increasing amounts of GSH in DMSO/bis-tris buffer (8/2, v/v). Inset: Absorption at 382 nm versus the number of equiv of GSH added.

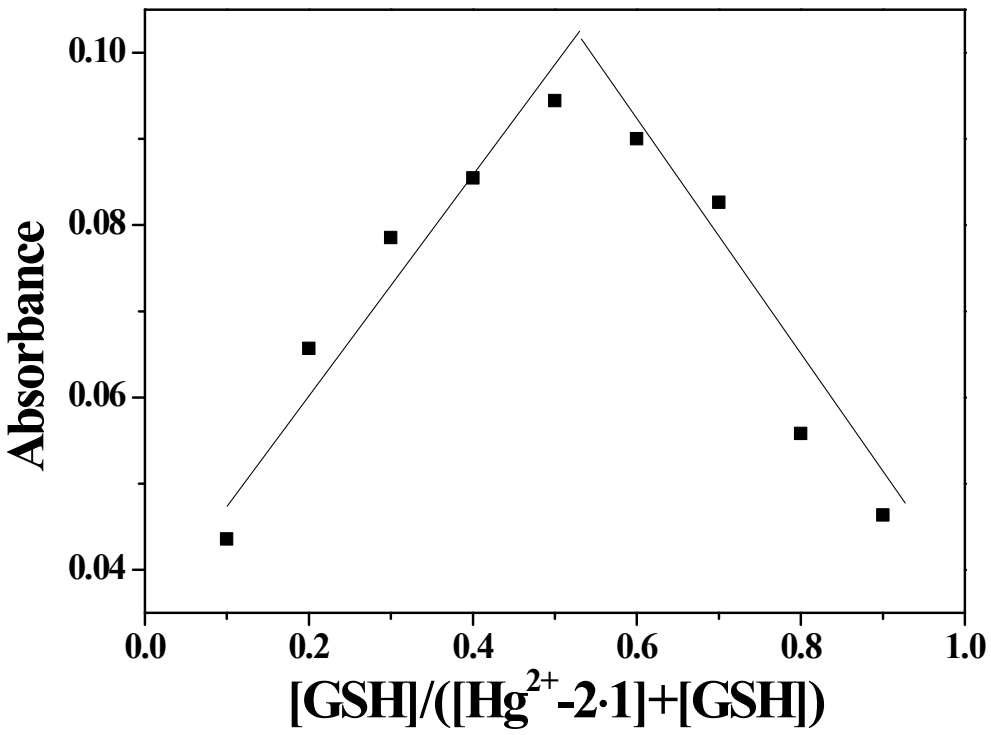

Fig. S13 Job plot for the binding of Hg^{2+}-2·**1** with Cys. Absorbance at 382 nm was plotted as a function of the molar ratio [GSH]/([Hg^{2+}-2·**1**] + [GSH]). The total concentrations of Cys with Hg^{2+}-2·**1** were 10 μM.

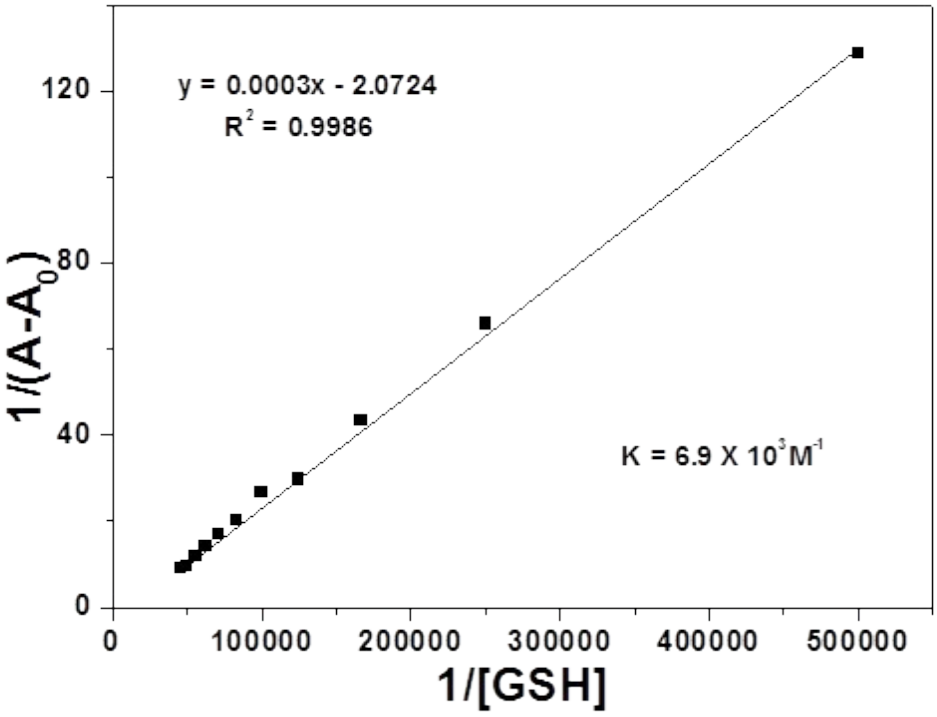

Fig. S14 Benesi-Hildebrand plot (absorbance at 382 nm) of **1**, assuming a 1:1 stoichiometry for association between Hg^{2+}-2·**1** and GSH.

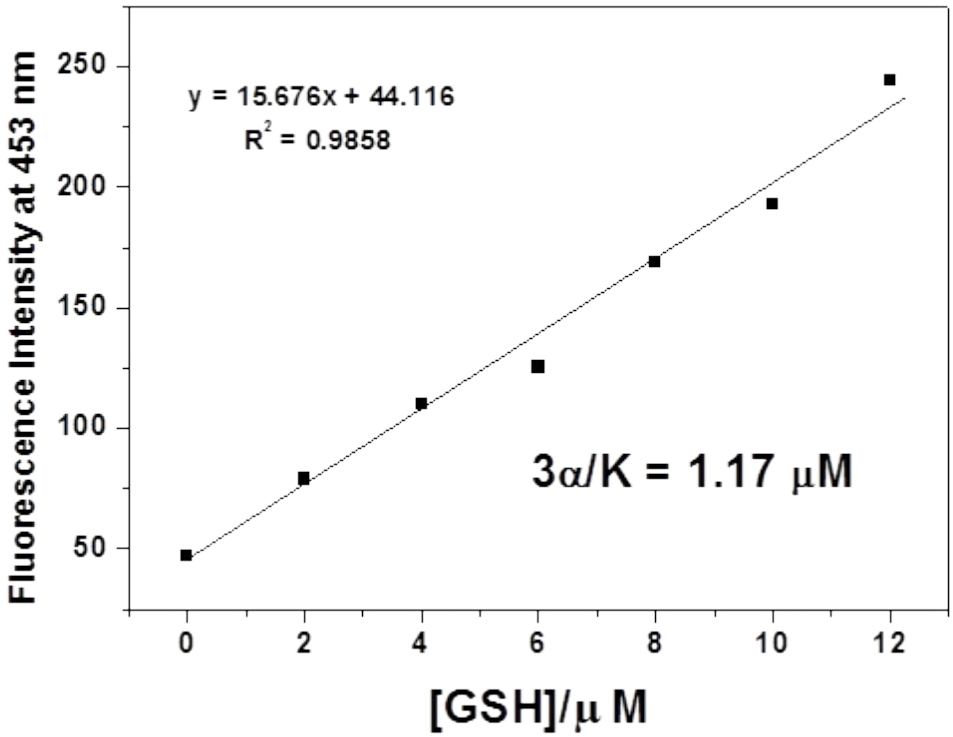

Fig. S15 Determination of the detection limit based on change in the ratio (absorbance at 453 nm) of Hg^{2+}-2·**1** (10 μM) with GSH.

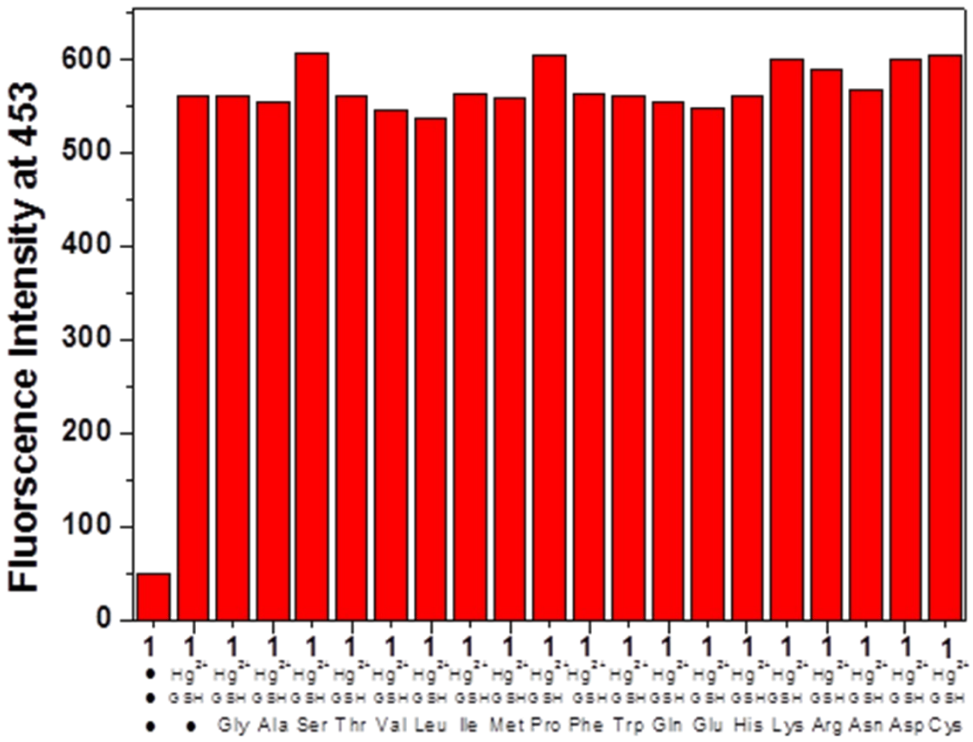

Fig. S16 Competitive selectivity of Hg^{2+}-2·**1** toward GSH (2 equiv) in the presence of other amino acids (2 equiv) in DMSO/bis-tris buffer (8/2, v/v).

(a)

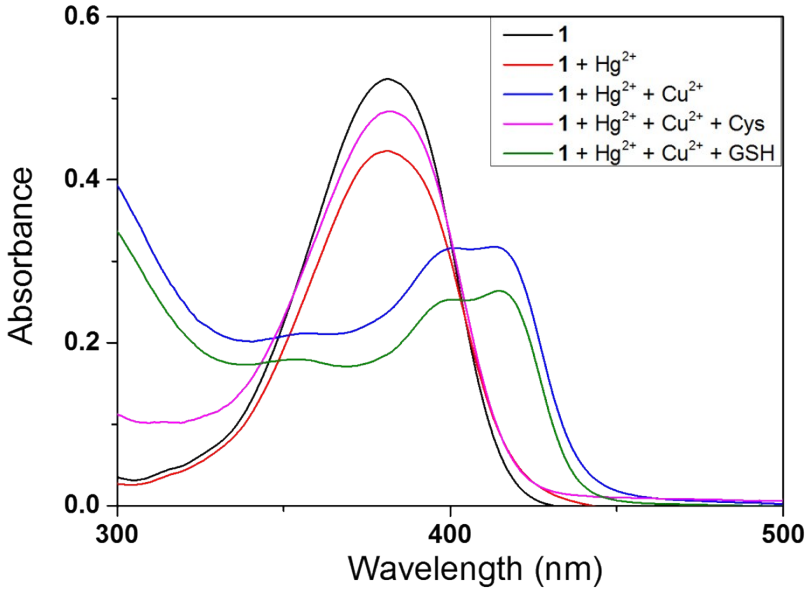

(b)

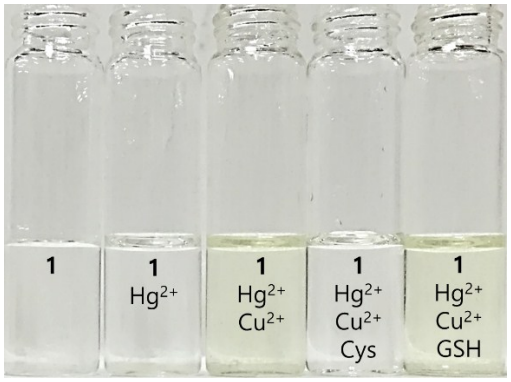

Fig. S17 (a) Changes in the UV-vis spectra of **1** (10 μM), **1**-Hg^{2+} (1 equiv), **1**-Hg^{2+}-Cu^{2+} (1 equiv), **1**-Hg^{2+}-Cu^{2+} (1 equiv)-Cys (13 equiv), and **1**-Hg^{2+}-Cu^{2+} (1 equiv)-GSH (13 equiv), respectively. (b) Color changes of **1** (10 μM), **1**-Hg^{2+} (1 equiv), **1**-Hg^{2+}-Cu^{2+} (1 equiv), **1**-Hg^{2+}-

Cu^{2+} (1 equiv)-Cys (13 equiv), and **1**-Hg^{2+}-Cu^{2+} (1 equiv)-GSH (13 equiv), respectively.

(a)

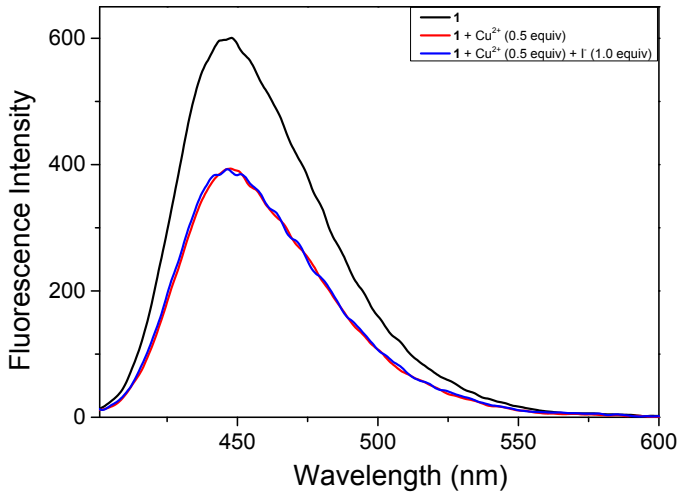

(b)

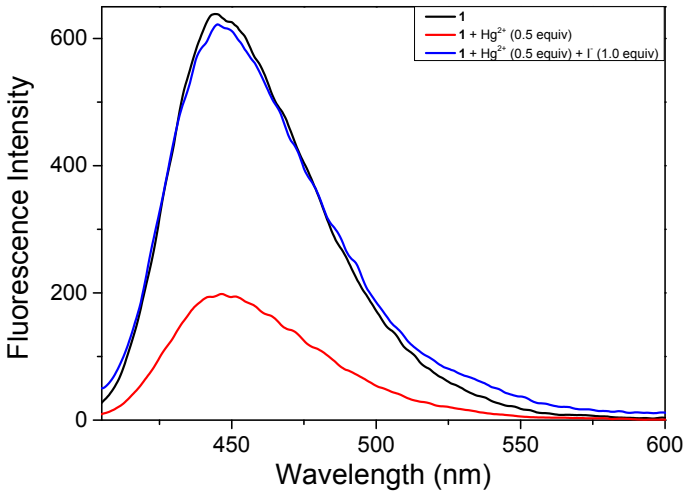

Fig. S18 Recovery tests of **1** with (a) **1**-Cu^{2+} (0.5 equiv) complex and (b) **1**-Hg^{2+} (0.5 equiv) complex in presence of I^- in DMSO/bis-tris buffer (8/2, v/v).